PERGAMON

International Journal of Solids and Structures 40 (2003) 161–180

INTERNATIONAL JOURNAL OF SOLIDS and STRUCTURES

www.elsevier.com/locate/ijsolstr

Vibration analysis of laminated composite cylindrical panels via a meshfree approach

X. Zhao [a], K.M. Liew [a,*], T.Y. Ng [b]

[a] *Nanyang Centre for Supercomputing and Visualisation, School of Mechanical and Production Engineering, Nanyang Technological University, Nanyang Avenue, Singapore 639798, Singapore*

[b] *Institute of High Performance Computing, 1 Science Park Road, #01-01, The Capricorn, Singapore Science Park II, Singapore 117528, Singapore*

Received 30 July 2001; received in revised form 17 July 2002

Abstract

In this paper, the free vibration of laminated composite cylindrical panels is solved by the meshfree (meshless) approach. The reproducing kernel particle approximation is employed to model the two-dimensional displacement functions. The effects of the particle distribution and the size of the domain of influence, on the convergence behavior, are studied. This study examines in detail the effects of different boundary conditions on the frequency characteristics of the cylindrical panels. The effects of the curvature of the cylindrical panels as well as the lamination scheme, on the frequencies of the panels, are also investigated. The present results are verified by comparison against results available in the open literature, with very good agreement being attained.

Keywords: Free vibration analysis; Cylindrical panels; Meshless method; Boundary conditions; Laminated composite; Particle distribution

1. Introduction

The vibration of cylindrical panels has been investigated by many researchers using various methods. Leissa (1993) presented the free vibration analysis of cylindrical panels with different boundary conditions based on the Donnell–Mushtari theory. The free vibration of a homogeneous isotropic thick cylindrical panel subjected to a certain type of simply supported edge boundary condition was analyzed by Soldatos and Hadjigeorgiou (1990) employing an iterative approach to solve the governing equations of three-dimensional linear elasticity. Bardell et al. (1997) conducted a comprehensive vibration study of thin, laminated, cylindrically curved shell panels using the *h–p* version of the finite element method. The free vibration analysis of cross-ply laminated shear deformable circular cylinders on the basis of orthogonal polynomials was presented by Soldatos (1984). The vibration of completely free composite plates and cylindrical shell panels by a

* Correspondence author. Tel.: +65-790-4076; fax: +65-793-6763.
E-mail address: mkmliew@ntu.edu.sg (K.M. Liew).

0020-7683/02/$ - see front matter
PII: S0020-7683(02)00475-4

higher-order theory based on orthogonal polynomials was provided by Messina and Soldatos (1999). Soldatos and Messina (2001) also discussed the influence of the edge boundary conditions on the vibration characteristics of transverse shear deformable composite open cylindrical panels having arbitrary angle-ply lay-up. Recently, Liew et al. (2000) and Liew and Feng (2000) presented the three-dimensional elasticity solutions to the free vibration problem of thick cylindrical and conical shell panels.

Meshless methods developed in recent years have become popular in computational mechanics and are applied in many areas. Nagashima (1999) presented the node-by-node meshless method for structural analysis. The element free method was provided by Ouatouati and Johnson (1999) for the modal analysis of free vibration of beams and plates. These methods do not require the need for a mesh in the formulation, and essentially only involve a number of nodal points. The reproducing kernel particle method (RKPM), developed by Liu et al. (1995a), is one meshless method, which takes full advantage of the concept of having no mesh. The RKPM is similar to smooth particle hydrodynamics (see Lucy, 1977 and Monaghan, 1988) in the sense that its formation initiates from the kernel estimate of a function. The difference is that the RKPM modifies the kernel function through the introduction of a correction function thereby enhancing its accuracy on or near the boundaries of the problem domain. As a result, the kernel function of the RKPM achieves consistency conditions across the domain of the problem. The mathematical aspects of meshless methods have been investigated with particular emphasis on RKPM by Liu et al. (1997) and Li and Liu (1996). This method provides a general formulation for the construction of shape functions for meshless computation, and has been applied in many fields by various researchers. Liu et al. (1995b) studied the applicability of the RKPM to structural dynamics, and the large deformation analysis of nonlinear structures was presented by Chen et al. (1996). The RKPM was also employed for modeling of human proximal femur (Liew et al., 2002a), elasto-plasticity (Liew et al., 2002b) and large deformation problems (Liew et al., 2002c). In order to investigate the dynamic behavior of rotating shells, Liew et al. (2002d) has proposed the harmonic reproducing kernel particle method and showed that it can produce excellent results for this problem.

In the Ritz method, we first have to search for admissible displacement functions that satisfy different combinations of boundary conditions, and therefore the eigen-value equations for the panels must be re-evaluated for each boundary condition case. In the present study, we employ two-dimensional reproducing kernel functions in the Ritz method to analyze the vibration of laminated composite cylindrical panels. In this meshfree approach (MFA), only one shape function type needs to be chosen to describe the interior domain. To cater for different boundary conditions, only the variational line integral (see Eqs. (33) and (36)) need to be re-evaluated. Another purpose for the use of the reproducing kernel particle approximation to model the two-dimensional displacement field is to overcome the deficiencies of two-dimensional harmonic functions, which are unable to capture the bending-extension stiffness terms in laminated composite panels. Due to the orthogonal nature of the harmonic functions, the B_{16} and B_{26} terms vanish during the analysis, which is appropriate for general cross-ply laminates, but incorrectly reflects the stiffness characteristics in angle-ply laminates. The present method is verified by comparing present results with those available in open literature.

2. Meshless formulation for panels

2.1. Energy formulation for the cylindrical panels

The cylindrical panel considered is as shown in Fig. 1a, where a coordinate system (x, θ, z) is fixed on the middle surface of the panel. This panel is considered to be thin and of length L, radius R and thickness h bounded along its edges by the lines $x = 0$, $x = L$, $\theta = 0$ and $\theta = \theta_0$. The displacements of the panel in the x-, θ-, and z-directions are denoted by u, v and w respectively. The kinetic energy for the cylindrical panels can be expressed as

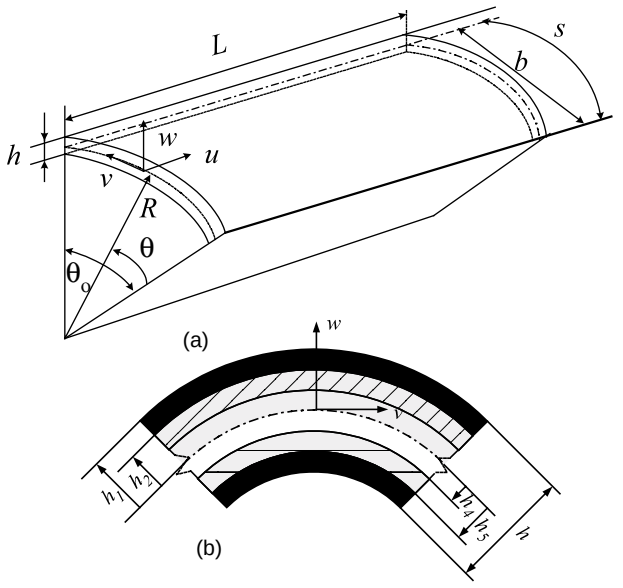

Fig. 1. (a) Coordinate system of the cylindrical panel. (b) Cross-sectional view of the laminated cylindrical panel.

$$T = \frac{1}{2}\rho h \int_0^L \int_0^{\theta_0} [\dot{u}^2 + \dot{v}^2 + \dot{w}^2] R \, \mathrm{d}\theta \, \mathrm{d}x \tag{1}$$

where the three terms are due to contributions from the linear velocities in the x-, θ-, and z-directions, respectively. The strain energy of the shell is given by

$$U_\varepsilon = \frac{1}{2} \int_0^L \int_0^{\theta_0} \varepsilon^{\mathrm{T}} [S] \varepsilon R \, \mathrm{d}\theta \, \mathrm{d}x \tag{2}$$

where ε^{T} and $[S]$ are the strain vector and stiffness matrix, respectively, and ε^{T} can be defined as

$$\varepsilon^{\mathrm{T}} = \{ e_1 \quad e_2 \quad \gamma \quad \kappa_1 \quad \kappa_2 \quad 2\tau \} \tag{3}$$

where the middle surface strains, e_1, e_2 and γ, and the middle surface curvatures, κ_1, κ_2 and τ, are defined according to Love's thin shell theory

$$e_1 = \frac{\partial u}{\partial x} \quad e_2 = \frac{1}{R}\left(\frac{\partial v}{\partial \theta} + w\right) \quad \gamma = \frac{\partial v}{\partial x} + \frac{1}{R}\frac{\partial u}{\partial \theta} \quad \kappa_1 = -\frac{\partial^2 w}{\partial^2 x} \quad \kappa_2 = -\frac{1}{R^2}\left(\frac{\partial^2 w}{\partial^2 \theta} - \frac{\partial v}{\partial \theta}\right)$$
$$\tau = -\frac{1}{R}\left(\frac{\partial^2 w}{\partial x \, \partial \theta} - \frac{\partial v}{\partial x}\right) \tag{4}$$

and $[S]$ is given by

$$[S] = \begin{bmatrix} A_{11} & A_{12} & A_{16} & B_{11} & B_{12} & B_{16} \\ A_{12} & A_{22} & A_{26} & B_{12} & B_{22} & B_{26} \\ A_{16} & A_{26} & A_{66} & B_{16} & B_{26} & B_{66} \\ B_{11} & B_{12} & B_{16} & D_{11} & D_{12} & D_{16} \\ B_{12} & B_{22} & B_{26} & D_{12} & D_{22} & D_{26} \\ B_{16} & B_{26} & B_{66} & D_{16} & D_{26} & D_{66} \end{bmatrix} \tag{5}$$

where the extensional (A_{ij}), coupling (B_{ij}) and bending (D_{ij}) stiffnesses, are defined as

$$(A_{ij}, B_{ij}, D_{ij}) = \int_{-h/2}^{h/2} Q_{ij}(1, z, z^2)\,\mathrm{d}z \tag{6}$$

and for a panel composed of different layers of orthotropic materials, the stiffnesses can be defined as

$$A_{ij} = \sum_{k=1}^{N_l} \overline{Q}_{ij}^{k}(h_k - h_{k+1}) \quad B_{ij} = \frac{1}{2}\sum_{k=1}^{N_l} \overline{Q}_{ij}^{k}(h_k^2 - h_{k+1}^2) \quad D_{ij} = \frac{1}{3}\sum_{k=1}^{N_l} \overline{Q}_{ij}^{k}(h_k^3 - h_{k+1}^3) \tag{7}$$

where h_k and h_{k+1} denote the distances from the panel reference surface to the outer and inner surfaces of the kth layer, respectively, as shown in Fig. 1b. N_l denotes the total number of layers in the laminated panel and $\overline{Q}_{ij}^{k}$ is the transformed reduced stiffness matrix for the kth layer defined as

$$[\overline{Q}] = [T]^{-1}[Q][T]^{-\mathrm{T}} \tag{8}$$

where $[T]$ is the transformation matrix for the principle material coordinates and the panel's coordinates, and is defined as

$$[T] = \begin{bmatrix} \cos^2\alpha & \sin^2\alpha & 2\cos\alpha\sin\alpha \\ \sin^2\alpha & \cos^2\alpha & -2\cos\alpha\sin\alpha \\ -\cos\alpha\sin\alpha & \cos\alpha\sin\alpha & \cos^2\alpha - \sin^2\alpha \end{bmatrix} \tag{9}$$

where α is the angular orientation of the fibres and $[Q]$ is the reduced stiffness matrix defined as

$$[Q] = \begin{bmatrix} Q_{11} & Q_{12} & 0 \\ Q_{12} & Q_{22} & 0 \\ 0 & 0 & Q_{66} \end{bmatrix} \tag{10}$$

The material constants in the reduced stiffness matrix $[Q]$ are given as

$$Q_{11} = \frac{E_{11}}{1 - v_{12}v_{21}} \quad Q_{12} = \frac{v_{12}E_{22}}{1 - v_{12}v_{21}} \quad Q_{22} = \frac{E_{22}}{1 - v_{12}v_{21}} \quad Q_{66} = G_{12} \tag{11}$$

where E_{11} and E_{22} are the elastic moduli in the principle material coordinates, G_{12} is the shear modulus and v_{12} and v_{21} are Poisson's ratio. The total energy functional of the panel is thus

$$\Gamma_t = T - U_\varepsilon \tag{12}$$

2.2. Two-dimensional reproducing kernel particle shape functions and their derivatives for cylindrical panels

The discrete displacement approximations for shell panels take the form

$$u(x,\theta) = \sum_{I=1}^{\mathrm{NP}} \Psi_I(x,\theta)u_I\mathrm{e}^{\mathrm{i}\omega t} \quad v(x,\theta) = \sum_{I=1}^{\mathrm{NP}} \Psi_I(x,\theta)v_I\mathrm{e}^{\mathrm{i}\omega t} \quad w(x,\theta) = \sum_{I=1}^{\mathrm{NP}} \Psi_I(x,\theta)w_I\mathrm{e}^{\mathrm{i}\omega t} \tag{13}$$

where NP is the total number of particles and $\Psi_I(x,\theta)$'s are the shape functions of displacements u, v, and w. The 2D shape function is expressed as

$$\boldsymbol{\Psi}_I(\boldsymbol{x};\boldsymbol{x}-\boldsymbol{x}_I) = \boldsymbol{C}(\boldsymbol{x};\boldsymbol{x}-\boldsymbol{x}_I)\boldsymbol{\Phi}_a(\boldsymbol{x}-\boldsymbol{x}_I) \tag{14}$$

where $\boldsymbol{C}(\boldsymbol{x};\boldsymbol{x}-\boldsymbol{x}_I)$ is the correction function and $\boldsymbol{\Phi}_a(\boldsymbol{x}-\boldsymbol{x}_I)$ is the weight function. The correction function $\boldsymbol{C}(\boldsymbol{x};\boldsymbol{x}-\boldsymbol{x}_I)$ is described as

$$\begin{aligned}
&\boldsymbol{C}(\boldsymbol{x};\boldsymbol{x}-\boldsymbol{x}_I)=\boldsymbol{H}^{\mathrm{T}}(\boldsymbol{x}-\boldsymbol{x}_I)\boldsymbol{b}(\boldsymbol{x})\\
&\boldsymbol{b}(\boldsymbol{x})=[b_0(x,\theta),b_1(x,\theta),b_2(x,\theta),b_3(x,\theta),b_4(x,\theta),b_5(x,\theta)]^{\mathrm{T}}\\
&\boldsymbol{H}(\boldsymbol{x}-\boldsymbol{x}_I)=[1,x-x_I,\theta-\theta_I,(x-x_I)(\theta-\theta_I),(x-x_I)^2,(\theta-\theta_I)^2]^{\mathrm{T}}
\end{aligned}\tag{15}$$

$\boldsymbol{H}$ is a vector of quadratic basis and $b_i(x,\theta)$'s are functions of x and θ which are to be determined. Thus, the shape function can be written as

$$\boldsymbol{\Psi}_I(\boldsymbol{x})=\boldsymbol{b}^{\mathrm{T}}(\boldsymbol{x})\boldsymbol{H}(\boldsymbol{x}-\boldsymbol{x}_I)\boldsymbol{\Phi}_a(\boldsymbol{x}-\boldsymbol{x}_I)\tag{16}$$

Eq. (16) can be rewritten as

$$\boldsymbol{\Psi}_I(\boldsymbol{x})=\boldsymbol{b}^{\mathrm{T}}(\boldsymbol{x})\boldsymbol{B}_I(\boldsymbol{x}-\boldsymbol{x}_I)\tag{17}$$

where

$$\begin{aligned}
&\boldsymbol{b}(\boldsymbol{x})=\boldsymbol{M}^{-1}(\boldsymbol{x})\boldsymbol{H}(\boldsymbol{0})\\
&\boldsymbol{B}_I(\boldsymbol{x}-\boldsymbol{x}_I)=\boldsymbol{H}(\boldsymbol{x}-\boldsymbol{x}_I)\boldsymbol{\Phi}_a(\boldsymbol{x}-\boldsymbol{x}_I)
\end{aligned}\tag{18}$$

and the moment matrix $\boldsymbol{M}$ is a function of $\boldsymbol{x}$ while $\boldsymbol{H}(\boldsymbol{0})$ is a constant vector. The expressions of $\boldsymbol{M}$ and $\boldsymbol{H}(\boldsymbol{0})$ are given by

$$\boldsymbol{M}(\boldsymbol{x})=\sum_{I=1}^{\mathrm{NP}}\boldsymbol{H}(\boldsymbol{x}-\boldsymbol{x}_I)\boldsymbol{H}^{\mathrm{T}}(\boldsymbol{x}-\boldsymbol{x})\boldsymbol{\Phi}_a(\boldsymbol{x}-\boldsymbol{x}_I)\tag{19}$$

$$\boldsymbol{H}(\boldsymbol{0})=[1,0,0,0,0,0]\tag{20}$$

The shape function can therefore be expressed as

$$\boldsymbol{\Psi}_I(\boldsymbol{x})=\boldsymbol{H}^{\mathrm{T}}(\boldsymbol{0})\boldsymbol{M}^{-1}(\boldsymbol{x})\boldsymbol{H}(\boldsymbol{x}-\boldsymbol{x}_I)\boldsymbol{\Phi}_a(\boldsymbol{x}-\boldsymbol{x}_I)\tag{21}$$

For this thin shell problem, the first and second derivatives of the shape function need to be determined. Eq. (18) can be rewritten as

$$\boldsymbol{M}(\boldsymbol{x})\boldsymbol{b}(\boldsymbol{x})=\boldsymbol{H}(\boldsymbol{0})\tag{22}$$

The vector $\boldsymbol{b}(\boldsymbol{x})$ can be determined using LU decomposition of the matrix $\boldsymbol{M}(\boldsymbol{x})$ followed by backward substitution. The derivatives of $\boldsymbol{b}(\boldsymbol{x})$ can be obtained similarly. Taking the derivative of Eq. (22), we have

$$\boldsymbol{M}_{,x}(\boldsymbol{x})\boldsymbol{b}(\boldsymbol{x})+\boldsymbol{M}(\boldsymbol{x})\boldsymbol{b}_{,x}(\boldsymbol{x})=\boldsymbol{H}_{,x}(\boldsymbol{0})\tag{23}$$

which can be rearranged as

$$\boldsymbol{M}(\boldsymbol{x})\boldsymbol{b}_{,x}(\boldsymbol{x})=\boldsymbol{H}_{,x}(\boldsymbol{0})-\boldsymbol{M}_{,x}(\boldsymbol{x})\boldsymbol{b}(\boldsymbol{x})\tag{24}$$

It can be seen that the first derivative of $\boldsymbol{b}(\boldsymbol{x})$ can be formulated using the LU decomposition procedure again. The second derivative of $\boldsymbol{b}(\boldsymbol{x})$ can be determined by taking derivative of Eq. (24) and using the same LU decomposition procedure. The first derivative of the shape function can be obtained by taking the derivative of Eq. (17)

$$\boldsymbol{\Psi}_{I,x}(\boldsymbol{x})=\boldsymbol{b}_{,x}^{\mathrm{T}}(\boldsymbol{x})\boldsymbol{B}_I(\boldsymbol{x}-\boldsymbol{x}_I)+\boldsymbol{b}^{\mathrm{T}}(\boldsymbol{x})\boldsymbol{B}_{I,x}(\boldsymbol{x}-\boldsymbol{x}_I)\tag{25}$$

and the second derivative of the shape function can be calculated again by taking derivative of Eq. (25)

$$\boldsymbol{\Psi}_{I,xx}(\boldsymbol{x})=\boldsymbol{b}_{,xx}^{\mathrm{T}}(x)\boldsymbol{B}_I(\boldsymbol{x}-\boldsymbol{x}_I)+2\boldsymbol{b}_{,x}^{\mathrm{T}}(\boldsymbol{x})\boldsymbol{B}_{I,x}(\boldsymbol{x}-\boldsymbol{x}_I)+\boldsymbol{b}^{\mathrm{T}}(\boldsymbol{x})\boldsymbol{B}_{I,xx}(\boldsymbol{x}-\boldsymbol{x}_I)\tag{26}$$

In this work, the cubic spline function is chosen as the weight function. Thus for this two-dimensional problem, the shape function is expressed by

$$\varphi(x,\theta) = \phi_x(x)\cdot\phi_\theta(\theta) \tag{27}$$

where

$$\phi_z(z_I) = \left\{ \begin{array}{ll} \frac{2}{3} - 4z_I^2 + 4z_I^3 & \text{for } 0 \leqslant |z_I| \leqslant \frac{1}{2} \\ \frac{4}{3} - 4z_I + 4z_I^2 - \frac{4}{3}z_I^3 & \text{for } \frac{1}{2} \leqslant |z_I| \leqslant 1 \\ 0 & \text{otherwise} \end{array} \right\} \quad z_I = \frac{(x - x_I)}{d} \tag{28}$$

where the dilatation parameter, d, is the size of the support. At a node, the size of the domain of influence is calculated by

$$d_I = d_{\max} a_I \tag{29}$$

where $d_{\max}$ is a scaling factor which ranges from 2.0 to 4.0. The distance a_I is determined by searching for enough nodes to avoid singularity of the matrix M.

In order to compute the derivatives of the shape function, it is necessary to determine the derivatives of the weight function. The first and second derivatives of the weight function can be easily obtained using the chain rule

$$\frac{\mathrm{d}\phi}{\mathrm{d}x} = \frac{\mathrm{d}\phi}{\mathrm{d}z}\frac{\mathrm{d}z}{\mathrm{d}x} = \left\{ \begin{array}{ll} (-8z_I + 12z_I^2)\mathrm{sign}(x - x_I) & \text{for } 0 \leqslant |z_I| \leqslant \frac{1}{2} \\ (-4 + 8z_I - 4z_I^2)\mathrm{sign}(x - x_I) & \text{for } \frac{1}{2} \leqslant |z_I| \leqslant 1 \\ 0 & \text{otherwise} \end{array} \right\} \tag{30}$$

$$\frac{\mathrm{d}^2\phi}{\mathrm{d}x^2} = \frac{\mathrm{d}^2\phi}{\mathrm{d}z^2}\left(\frac{\mathrm{d}z}{\mathrm{d}x}\right)^2 = \left\{ \begin{array}{ll} (-8 + 24z_I) & \text{for } 0 \leqslant |z_I| \leqslant \frac{1}{2} \\ (8 - 8z_I) & \text{for } \frac{1}{2} \leqslant |z_I| \leqslant 1 \\ 0 & \text{otherwise} \end{array} \right\} \tag{31}$$

It is noted that the first and second derivatives of the weight function are continuous over the entire domain.

2.3. Matrix equation for panels

It is necessary to correctly enforce the different boundary conditions in order to accurately solve the problem. There are several approaches to enforce essential boundary conditions in meshless methods, such as the Lagrange multiplier approach, modified variational principles, etc. In the present work, the penalty method is utilized to implement essential boundary conditions. The penalty formulation is developed as follows:

2.3.1. Simply supported boundary conditions

For the domain bounded by l_u, the displacement boundary condition is

$$\mathbf{u} = \bar{\mathbf{u}} \quad \text{on } l_u \tag{32}$$

in which $\bar{\mathbf{u}}$ is the prescribed displacement on the displacement boundary l_u. The variational form is given by

$$\Gamma_{\bar{u}} = \frac{\alpha}{2}\int_{l_u} (\mathbf{u} - \bar{\mathbf{u}})^{\mathrm{T}}(\mathbf{u} - \bar{\mathbf{u}})\,\mathrm{d}l \tag{33}$$

where α is the penalty parameter taken as $10^3 E_{11}$, with E_{11} being the elastic modulus of the shell in the principal coordinate direction.

2.3.2. Clamped boundary conditions

In the clamped case, for the domain bounded by l_u, besides the boundary condition described by Eq. (33), the rotation boundary condition is also included

$$\beta = \bar{\beta} \quad \text{on } l_u \tag{34}$$

where

$$\beta = \frac{\mathrm{d}w}{\mathrm{d}x} \tag{35}$$

and $\bar{\beta}$ is the prescribed rotation on the boundary. The variational form due to the rotation is expressed as

$$\Gamma_{\bar{\beta}} = \frac{\alpha}{2}\int_{l_u} (\beta - \bar{\beta})^{\mathrm{T}}(\beta - \bar{\beta})\,\mathrm{d}l \tag{36}$$

Therefore, the variational form due to the boundary conditions can be expressed as

$$\Gamma_B = \Gamma_{\bar{u}} + \Gamma_{\bar{\beta}} \tag{37}$$

and the total energy functional for this problem is thus

$$\Gamma = \Gamma_t + \Gamma_B \tag{38}$$

Substituting the displacement functions of Eq. (13) into the total energy functional of Eq. (38) and applying the Rayleigh–Ritz minimization procedure

$$\frac{\partial \Gamma}{\partial \Delta} = 0, \quad \Delta = u_I, v_I, w_I \quad I = 1, 2, \ldots, \mathrm{NP} \tag{39}$$

From Eqs. (38) and (39), applying Hamilton's principle, the following eigen-equation for the panels can be derived

$$(\widetilde{K} - \omega^2 \widetilde{M})\hat{\boldsymbol{u}} = 0 \tag{40}$$

where

$$\widetilde{K} = \Lambda^{-1} K \Lambda^{-\mathrm{T}} \tag{41}$$

$$\widetilde{M} = \Lambda^{-1} M \Lambda^{-\mathrm{T}} \tag{42}$$

$$\hat{\boldsymbol{u}} = [\hat{u}_1, \hat{v}_1, \hat{w}_1, \hat{u}_2, \hat{v}_2, \hat{w}_2, \ldots, \hat{u}_{\mathrm{NP}}, \hat{v}_{\mathrm{NP}}, \hat{w}_{\mathrm{NP}}] \tag{43}$$

and

$$K = K^{\varepsilon} + K^{B_1} + K^{B_2} \tag{44}$$

K^{ε} is the stiffness matrices due to the strain, while K^{B_1} and K^{B_2} are stiffnesses due to the boundary conditions.

$$\Lambda_{IJ} = \Psi_I(x_J)\boldsymbol{I}, \quad \boldsymbol{I} \text{ is the identity matrix} \tag{45}$$

$$K^{\varepsilon}_{IJ} = R\int_0^L \int_0^{\theta_0} B^{\varepsilon\mathrm{T}}_I [S] B^{\varepsilon}_J \,\mathrm{d}x\,\mathrm{d}\theta \tag{46}$$

$$K^{B_1}_{IJ} = \alpha\rho h R\left(\int_{\Gamma_U} B1^{B^{\mathrm{T}}}_I B^B_J \,\mathrm{d}l + \int_{\Gamma_U} B1^B_I \bar{\mathbf{u}}\,\mathrm{d}l\right) \tag{47}$$

$$K^{B_2}_{IJ} = \alpha\rho h R\left(\int_{\Gamma_U} B2^{B^{\mathrm{T}}}_I B^B_J \,\mathrm{d}l + \int_{\Gamma_U} B2^B_I \bar{\beta}\,\mathrm{d}l\right) \tag{48}$$

$$M = \rho h R \int_0^L \int_0^{\theta_0} M_I^{\mathrm{T}} M_J \,\mathrm{d}x \,\mathrm{d}\theta \tag{49}$$

$$[B_I^{\varepsilon}] = \begin{bmatrix} \dfrac{\partial \Psi_I}{\partial x} & 0 & 0 \\ 0 & \dfrac{1}{R}\dfrac{\partial \Psi_I}{\partial \theta} & \dfrac{\Psi_I}{R} \\ -\dfrac{1}{R}\dfrac{\partial \Psi_I}{\partial \theta} & \dfrac{\partial \Psi_I}{\partial x} & 0 \\ 0 & 0 & -\dfrac{\partial^2 \Psi_I}{\partial x^2} \\ 0 & \dfrac{1}{R^2}\dfrac{\partial \Psi_I}{\partial \theta} & \dfrac{1}{R^2}\dfrac{\partial^2 \Psi_I}{\partial \theta^2} \\ 0 & \dfrac{2}{R}\dfrac{\partial \Psi_I}{\partial x} & \dfrac{2}{R}\dfrac{\partial^2 \Psi_I}{\partial x \partial \theta} \end{bmatrix} \tag{50}$$

$$B1_I^B = \begin{bmatrix} \Psi_I & 0 & 0 \\ 0 & \Psi_I & 0 \\ 0 & 0 & \Psi_I \end{bmatrix} \quad B2_I^B = \begin{bmatrix} \Psi_{I,x} & 0 & 0 \\ 0 & \Psi_{I,x} & 0 \\ 0 & 0 & \Psi_{I,x} \end{bmatrix} \tag{51}$$

$$M = \begin{bmatrix} \Psi_I & 0 & 0 \\ 0 & \Psi_I & 0 \\ 0 & 0 & \Psi_I \end{bmatrix} \tag{52}$$

3. Numerical results and discussion

3.1. Comparison and convergence studies

In order to verify the present approach and to examine the accuracy of the method, numerical results are compared with those existing in open literature. Table 1 shows comparisons of frequency parameter $\bar{\omega} = \omega L\sqrt{\rho(1+v)/E}$ for isotropic simply supported circular cylindrical panels with solutions given by Soldatos and Hadjigeorgiou, 1990. The results tabulated in Table 1 provide an insight to the convergence characteristics of the present methodology when the support sizes increase from 2.5 to 3.5 and the number of particles increase from 8×8 to 14×14. It can be seen that the fundamental frequencies converge, in a monotonic manner, with the increases of the support size and the number of nodes. It is also observed that the good agreement is obtained between the present results with those given by Soldatos and Hadjigeorgiou (1990) based on the Sanders (SDST) and Flügge (CST) theories, for thin panels ($h/b \leqslant 0.1$). For relatively thick cylindrical panels ($h/b \geqslant 0.2$), the present results are higher than those based on the Sanders (SDST) and lower than those obtained through Flügge (CST), which are considered to be less accurate. For a two-layer [90°/0°] simply supported circular cylindrical panel, the present results of frequency parameter $\hat{\omega} = \omega s^2\sqrt{\rho/E_2 h^2}$ are compared in Table 2 with those results provided by Bardell et al. (1997), Soldatos (1984) and Bercin (1996). It is observed that the convergent results can be achieved using relatively less nodes (10×10) and smaller support size ($d = 2.5$). Table 3 shows comparisons of the first four frequency parameter $\tilde{\omega} = \omega L^2\sqrt{12\rho(1-v^2)/Eh^2}$ for a free isotropic cylindrical panel, with results provided by Leissa and Narita (1984) and Messina and Soldatos (1999). The maximum discrepancies for the four modes are 0.58%, 1.42%, 1.07% and 0.97%, respectively. The maximum discrepancies for the four modes between the

Table 1
Comparison of frequency parameter $\bar{\omega} = \omega L\sqrt{\rho(1+\nu)/E}$ for an isotropic simply supported circular cylindrical panel ($L/b = 1$, $\nu = 0.3$, $m = n = 1$)

h/b	θ_0	Soldatos and Hadjigeorgiou (1990)		Present meshless											
		Flügge CST	Sanders SDST	$d = 2.5$				$d = 3.0$				$d = 3.5$			
				8×8	10×10	12×12	14×14	8×8	10×10	12×12	14×14	8×8	10×10	12×12	14×14
0.1	30°	0.7207	0.7001	0.7149	0.7154	0.7158	0.7161	0.7099	0.7119	0.7132	0.7139	0.7094	0.7120	0.7135	0.7144
	60°	0.8262	0.8096	0.8101	0.8131	0.8149	0.8162	0.8033	0.8083	0.8113	0.8132	0.7993	0.8056	0.8094	0.8118
	90°	0.9696	0.9575	0.9435	0.9491	0.9525	0.9546	0.9347	0.9428	0.9476	0.9507	0.9271	0.9496	0.9433	0.9474
0.2	30°	1.3448	1.2033	1.3357	1.3349	1.3348	1.3348	1.3269	1.3289	1.3302	1.3311	1.3278	1.3307	1.3321	1.3330
	60°	1.3118	1.1979	1.2860	1.2873	1.2882	1.2889	1.2763	1.2806	1.2831	1.2848	1.2744	1.2800	1.2832	1.2852
	90°	1.3015	1.2199	1.2586	1.2625	1.2649	1.2665	1.2476	1.2548	1.2589	1.2617	1.2420	1.2511	1.2565	1.2601
0.3	30°	1.9803	1.5947	1.9595	1.9580	1.9575	1.9574	1.9471	1.9495	1.9510	1.9521	1.9489	1.9525	1.9542	1.9552
	60°	1.8362	1.5281	1.7824	1.7827	1.7831	1.7835	1.7701	1.7742	1.7767	1.7783	1.7692	1.7749	1.7779	1.7798
	90°	1.6937	1.4699	1.6138	1.6164	1.6181	1.6194	1.6007	1.6073	1.6113	1.6138	1.5963	1.6149	1.6100	1.6133

Table 2
Comparison of frequency parameter $\hat{\omega} = \omega s^2\sqrt{\rho/E_2h^2}$ for a two-layer [90°/0°] simply supported circular cylindrical panel ($s/R = 0.5$, $R/h = 40$)

L/s	Bardell et al. (1997)	Soldatos (1984)	Bercin (1996)	Present meshless											
				$d = 2.5$				$d = 3.0$				$d = 3.5$			
				8×8	10×10	12×12	14×14	8×8	10×10	12×12	14×14	8×8	10×10	12×12	14×14
1	11.69	11.84	12.01	11.4915	11.4731	11.464	11.4585	11.4895	11.4608	11.4488	11.4435	11.5192	11.4786	11.4621	11.4545
2	7.33	7.25	7.43	7.1727	7.1496	7.1366	7.1289	7.2485	7.1915	7.1623	7.1456	7.2926	7.2186	7.1826	7.1622
3	6.54	6.39	6.59	6.4264	6.3975	6.3809	6.3707	6.5091	6.4447	6.4112	6.3915	6.5517	6.4716	6.4317	6.4086
4	6.28	6.11	6.30	6.1866	6.1548	6.1364	6.1250	6.2537	6.1929	6.1611	6.1423	6.2856	6.2137	6.1777	6.1567
5	6.17	5.99	6.20	6.0859	6.0532	6.0341	6.0222	6.1271	6.0759	6.0489	6.0328	6.1449	6.0884	6.0594	6.0432

present results and those provided by Messina and Soldatos (1999) are respectively 1.52%, 2.38%, 1.50% and 0.13%. In Table 4, present solutions for the four-layer $[-60°/60°/60°/-60°]$ free circular cylindrical panels are compared with those provided Qatu and Leissa (1991), Messina and Soldatos (1999). It is observed that the present analysis shows good convergence characteristics and agree well with results of Qatu and Leissa (1991) and Messina and Soldatos (1999) for the first ten modes. For the free panels with different lamination schemes $[\phi/-\phi/\phi]$, comparisons between the present results using various nodal distributions and support sizes, and results of Messina and Soldatos (1999) and Qatu (1992), are tabulated in Table 5. Both these works used in the comparison were based on the energy functional of the classical shallow shell theory, and the present results show good agreement.

In order to study the effects of the curvature of the panel on the convergence characteristics of the present meshfree method, some comparisons for plates which can be considered as a special case of a panel, with $1/R = 0$, are performed and tabulated in Tables 6 and 7. For a free isotropic square plate, Table 6 compares the first four frequency parameters $\tilde{\omega} = \omega L^2\sqrt{12\rho(1-\nu^2)/Eh^2}$ with corresponding results of Leissa and Narita (1984) and Messina and Soldatos (1999), who employed Ritz method to predict the frequencies. Apart from good agreement, stable convergence characteristics are also observed. For the free laminated square plates with different lamination schemes $[\phi/-\phi/\phi]$, Table 7 shows the comparison of the frequency parameters $\hat{\omega} = \omega L^2\sqrt{\rho/E_1h^2}$ corresponding parameters predicted by Qatu (1991) and Messina and Soldatos (1999). Generally good agreement is observed. However, there exists some relatively large discrepancy between the results of Qatu (1991) and Messina and Soldatos (1999), for the seventh and eighth modes for the case where the lamination scheme is $[0/-0/0]$. Messina and Soldatos (1999) attributed this to possible numerical instabilities in the methods applied by Qatu (1991). However, the present methodology provides similar results with those given by Qatu (1991), and the present authors thus believe the disagreement is possibly caused by other reasons. From the comparisons documented in Tables 6 and 7, it is observed that the curvature of the panel does not affect the convergence characteristics of the present approach.

Figs. 2–5 show the effects of particle distribution and the size of the domain of influence on the convergence characteristics of the fundamental frequencies, of a free isotropic square panel. A frequency parameter of $\omega^* = \omega L^2\sqrt{12\rho(1-\nu^2)/Eh^2}$ is used here. Monotonic convergence behavior is observed. The corresponding numerical results for four modes are tabulated in Table 8. The number of points varies from 6×6 to 14×14, and the size of the domain of influence varies from 2.0 to 3.5. It can be seen from the Table 8 that for smaller sizes of the domain of influence, more points are required to obtain the converged results. Similarly, when the particle distribution is relatively dilute, convergence can still be achieved by increasing the size of the domain of influence. In the present work, for the sake of computational efficiency, a larger size of the domain of influence with lower number of particles is selected because less particles translates to reduced sizes of the characteristic matrices. For this particular case, the results can be considered converged when using 10×10 particles with the size of domain of influence being 3.5.

The variation of the frequencies, for the modes 1 and 3, of a simply supported isotropic square panel, with the particle distribution and the size of the domain of influence is presented in Table 9. Similar observations as those arising in Table 8 are also observed here. Further, in a relative comparison of these two tables, it is found that the boundary conditions also affect the convergence characteristics. Results involving free edges tend to converge faster than those involving simply supported edge conditions.

3.2. Parametric studies

The effects of the boundary conditions on the fundamental frequencies of the panels with different lamination schemes will now be examined in detail. Figs. 6–9 show the variation of the frequencies with the lamination scheme for simply supported (SSSS), cantilevered (CFFF), and free (FFFF) cylindrical panels

Table 3
Comparison of frequency parameter $\tilde{\omega} = \omega L^2\sqrt{12\rho(1-\nu^2)/Eh^2}$ for an isotropic free circular cylindrical panel ($L/R = 0.5$, $L/h = 100$, $L/b = 1$, $\nu = 0.3$)

Mode	Leissa and Narita (1984)	Messina and Soldatos (1999)	Present meshless											
			$d = 2.5$				$d = 3.0$				$d = 3.5$			
			8×8	10×10	12×12	14×14	8×8	10×10	12×12	14×14	8×8	10×10	12×12	14×14
1	13.508	13.346	13.6325	13.5946	13.5778	13.5688	13.5889	13.5692	13.5606	13.5563	13.5684	13.5577	13.5535	13.5516
2	22.073	21.473	22.3144	22.1644	22.0913	22.0495	22.1277	22.0520	22.0131	21.9924	22.0578	22.0263	22.0093	21.9967
3	34.868	34.201	35.0995	34.9362	34.8527	34.8026	34.8694	34.7891	34.7472	34.7226	34.8056	34.7623	34.7389	34.7224
4	48.703	48.877	49.2905	49.0605	48.9575	48.9003	48.9831	48.8801	48.8350	48.8101	48.9210	48.8575	48.8284	48.8100

Table 4
Comparison of frequency parameter $\hat{\omega} = \omega L^2\sqrt{\rho/E_1h^2}$ for a four-layer $[-60°/60°/60°/-60°]$ free circular cylindrical panel ($L/R = 0.5$, $L/h = 100$, $L/b = 1$)

Material	Mode	Qatu and Leissa (1991)	Messina and Soldatos (1999)	Present meshless											
				$d = 2.5$				$d = 3.0$				$d = 3.5$			
				8×8	10×10	12×12	14×14	8×8	10×10	12×12	14×14	8×8	10×10	12×12	14×14
E-glass/ epoxy	1	3.2920	3.2498	3.3259	3.3137	3.3086	3.3059	3.3131	3.3068	3.3042	3.3028	3.3069	3.3036	3.3023	3.3016
	2	5.7416	5.5910	5.8048	5.7669	5.7483	5.7376	5.7567	5.7373	5.7279	5.7227	5.7389	5.7311	5.7269	5.7328
	3	8.5412	8.3873	8.6113	8.5648	8.5422	8.5289	8.5472	8.5265	8.5156	8.5091	8.5313	8.5195	8.5131	8.5087
	4	11.114	11.137	11.2358	11.1872	11.1653	11.1529	11.1695	11.1482	11.1385	11.1330	11.1563	11.1434	11.1371	11.1331
	5	12.591	12.533	12.7924	12.7221	12.6874	12.6665	12.6797	12.6543	12.6391	12.6295	12.6606	12.6428	12.6329	12.6262
	6	15.696	15.328	16.2461	16.0269	15.9122	15.8412	15.8535	15.7727	15.7320	15.7066	15.8517	15.7802	15.7458	15.7243
	7	18.221	17.895	18.6642	18.4844	18.3911	18.3321	18.3374	18.2696	18.2355	18.2136	18.3559	18.2848	18.2515	18.2309
	8	22.058	22.072	22.6171	22.3958	22.2944	22.2350	22.2702	22.1838	22.1457	22.1228	22.2584	22.1822	22.1486	22.1292
	9	22.194	22.142	22.7033	22.5076	22.4162	22.3613	22.3703	22.3089	22.2753	22.2533	22.3810	22.3099	22.2763	22.2566
	10	25.871	26.036	25.9199	25.8867	25.8687	25.8556	25.8603	25.8442	25.8354	25.8298	25.8488	25.8376	25.8321	25.8284
Graphite/ epoxy	1	2.2156	2.1841	2.2538	2.2356	2.2288	2.2255	2.2369	2.2281	2.2245	2.2226	2.2283	2.2240	2.2221	2.2212
	2	5.1241	4.9999	5.2097	5.1659	5.1537	5.1309	5.1517	5.1289	5.1185	5.1128	5.1273	5.1190	5.1151	5.1122
	3	5.5678	5.5116	5.6521	5.6043	5.5839	5.5733	5.5931	5.5753	5.5660	5.5607	5.5757	5.5654	5.5603	5.5572
	4	7.6824	7.6068	7.8552	7.7798	7.7423	7.7209	7.7471	7.7132	7.6973	7.6884	7.7160	7.6983	7.6903	7.6851
	5	7.9914	7.9690	8.1808	8.1110	8.0782	8.0592	8.0774	8.0530	8.0389	8.0300	8.0547	8.0377	8.0289	8.0232
	6	12.551	12.374	12.9815	12.8153	12.7325	12.6818	12.7087	12.6453	12.6116	12.5900	12.6969	12.6352	12.6047	12.5866
	7	12.982	12.902	13.3493	13.1951	13.1208	13.0768	13.1016	13.0423	13.0151	12.9987	13.0787	13.0343	13.0129	12.9998
	8	13.997	14.020	14.2654	14.1596	14.1061	14.0729	14.0878	14.0475	14.0258	14.0112	14.0661	14.0333	14.0165	14.0060
	9	14.926	14.744	15.3684	15.1861	15.0951	15.0397	15.0567	14.9901	14.9571	14.9366	15.0341	14.9777	14.9530	14.9382
	10	17.194	17.115	17.5086	17.3423	17.2584	17.2063	17.2305	17.1621	17.1284	17.1071	17.1959	17.1621	17.133	17.0983

Table 5
Comparison of frequency parameter $\hat{\omega} = \omega L^2\sqrt{\rho/E_1 h^2}$ for free circular cylindrical panels with graphite/epoxy layers $[\phi/-\phi/\phi]$ ($L/R = 0.5$, $L/h = 100$, $L/b = 1$)

ϕ	Mode	Qatu (1992)	Messina and Soldatos (1999)	Present meshless											
				$d = 2.5$				$d = 3.0$				$d = 3.5$			
				8×8	10×10	12×12	14×14	8×8	10×10	12×12	14×14	8×8	10×10	12×12	14×14
0°	1	1.488	1.470	1.4994	1.4959	1.4944	1.4935	1.4955	1.4937	1.4929	1.4925	1.4940	1.4929	1.4924	1.4921
	2	1.644	1.599	1.6592	1.6489	1.6439	1.6411	1.6467	1.6413	1.6386	1.6372	1.6421	1.6398	1.6386	1.6376
	3	3.448	3.388	3.4634	3.4499	3.4432	3.4391	3.4435	3.4377	3.4344	3.4324	3.4409	3.4371	3.4348	3.4330
	4	4.546	4.437	4.6996	4.6382	4.6062	4.5864	4.5889	4.5667	4.5556	4.5485	4.5915	4.5708	4.5607	4.5545
	5	6.432	6.317	6.5472	6.4992	6.4745	6.4585	6.4552	6.4393	6.4307	6.4247	6.4721	6.4502	6.4395	6.4328
	6	8.898	8.906	9.0648	8.9937	8.9594	8.9338	8.9344	8.8947	8.8741	8.8611	8.9294	8.9048	8.8868	8.8740
30°	1	1.695	1.658	1.7276	1.7104	1.7032	1.6994	1.7119	1.7023	1.6979	1.6957	1.7036	1.6986	1.6963	1.6949
	2	2.990	2.940	3.0298	3.0129	3.0048	3.0002	3.0039	2.9978	2.9948	2.9931	2.9970	2.9956	2.9945	2.9936
	3	4.304	4.226	4.4315	4.3672	4.3382	4.3223	4.3400	4.3195	4.3079	4.3008	4.3289	4.3143	4.3060	4.3005
	4	6.611	6.510	6.7915	6.7114	6.6715	6.6476	6.6532	6.6247	6.6114	6.6033	6.6456	6.6237	6.6136	6.6073
	5	7.103	7.034	7.3237	7.2161	7.1697	7.1447	7.1702	7.1349	7.1187	7.1089	7.1465	7.1238	7.1128	7.1058
	6	8.734	8.693	8.9895	8.8799	8.8296	8.8010	8.8214	8.7845	8.7665	8.7553	8.7937	8.7723	8.7607	8.7528
60°	1	1.792	1.766	1.8491	1.8184	1.8093	1.8025	1.8220	1.8078	1.8022	1.7995	1.8083	1.8020	1.7992	1.7978
	2	4.683	4.639	4.8243	4.7446	4.7152	4.6972	4.7269	4.7019	4.6893	4.6822	4.7011	4.6879	4.6814	4.6776
	3	5.196	5.074	5.2835	5.2398	5.2176	5.2049	5.2236	5.2019	5.1918	5.1863	5.2009	5.1931	5.1893	5.1864
	4	6.880	6.844	7.1621	7.0385	6.9874	6.9558	6.9885	6.9506	6.9308	6.9189	6.9519	6.9285	6.9174	6.9102
	5	7.430	7.356	7.6653	7.5606	7.5134	7.4826	7.5111	7.4701	7.4518	7.4415	7.4709	7.4538	7.4455	7.4395
	6	11.05	10.95	11.5407	11.3262	11.2297	11.1763	11.2223	11.1498	11.1157	11.0952	11.1803	11.1244	11.0988	11.0836
90°	1	1.514	1.496	1.5263	1.5224	1.5224	1.5202	1.5222	1.5204	1.5197	1.5193	1.5207	1.5197	1.5193	1.5190
	2	4.514	4.529	4.5578	4.5389	4.5389	4.5272	4.5329	4.5260	4.5231	4.5215	4.5304	4.5256	4.5233	4.5219
	3	6.455	6.280	6.5174	6.4774	6.4576	6.4463	6.4683	6.4469	6.4366	6.4308	6.4501	6.4409	6.4360	6.4323
	4	6.757	6.751	6.8585	6.8269	6.8152	6.8038	6.8055	6.7966	6.7917	6.7886	6.8034	6.7967	6.7929	6.7902
	5	7.092	6.917	7.1488	7.1109	7.0933	7.0808	7.0963	7.0783	7.0691	7.0638	7.0824	7.0734	7.0687	7.0650
	6	9.197	9.248	9.4156	9.3205	9.2871	9.2610	9.2782	9.2451	9.2323	9.2253	9.2837	9.2522	9.2389	9.2316

Table 6
Comparison of frequency parameter $\tilde{\omega} = \omega L^2\sqrt{12\rho(1-\nu^2)/Eh^2}$ for a square isotropic plate with free edges ($\nu = 0.3$)

Mode	Leissa and Narita(1984)	Messina and Soldatos(1999)	Present meshless											
			$d = 2.5$				$d = 3.0$				$d = 3.5$			
			8×8	10×10	12×12	14×14	8×8	10×10	12×12	14×14	8×8	10×10	12×12	14×14
1	13.468	13.468	13.5259	13.5073	13.4961	13.4889	13.4947	13.4836	13.4782	13.4753	13.4803	13.4744	13.4722	13.4712
2	19.596	19.596	19.7681	19.7118	19.6799	19.6596	19.6479	19.6370	19.6285	19.6220	19.6316	19.6355	19.6335	19.6293
3	24.271	24.270	24.6027	24.4942	24.4324	24.3930	24.3719	24.3502	24.3334	24.3206	24.3419	24.3486	24.3439	24.3352
4	34.801	34.801	35.0813	35.0115	34.9620	34.9266	34.9278	34.8917	34.8686	34.8529	34.9068	34.8860	34.8712	34.8587

Table 7
Comparison of frequency parameter $\hat{\omega} = \omega L^2\sqrt{\rho/E_1 h^2}$ for a laminated square plate (graphite/epoxy, $[/\phi/ - \phi/\phi]$)

ϕ	Mode	Qatu (1991)	Messina and Soldatos (1999)	Present meshless											
				$d = 2.5$				$d = 3.0$				$d = 3.5$			
				8×8	10×10	12×12	14×14	8×8	10×10	12×12	14×14	8×8	10×10	12×12	14×14
0°	1	1.4910	1.4910	1.4953	1.4940	1.4931	1.4926	1.4930	1.4922	1.4918	1.4916	1.4923	1.4917	1.4914	1.4913
	2	1.6461	1.6461	1.6638	1.6581	1.6548	1.6527	1.6514	1.6503	1.6495	1.6488	1.6499	1.6503	1.6501	1.6496
	3	3.4596	3.4597	3.4838	3.4780	3.4738	3.4707	3.4710	3.4679	3.4658	3.4643	3.4706	3.4684	3.4667	3.4653
	4	4.5393	4.5394	4.6988	4.6461	4.6177	4.5996	4.5929	4.5757	4.5674	4.5620	4.5991	4.5828	4.5744	4.5689
	5	6.4266	6.4266	6.5409	6.5153	6.4952	6.4812	6.4687	6.4587	6.4527	6.4480	6.4862	6.4725	6.4630	6.4569
	6	6.4713	6.4713	6.5510	6.5182	6.5052	6.4970	6.4919	6.4876	6.4843	6.4816	6.4911	6.4877	6.4868	6.4850
	7	7.1317	6.9702	7.1979	7.1791	7.1672	7.1592	7.1512	7.1478	7.1449	7.1424	7.1476	7.1481	7.1470	7.1451
	8	9.0088	7.1317	9.0789	9.0482	9.0196	8.9950	8.9735	8.9437	8.9263	8.9144	8.9804	8.9620	8.9446	8.9312
15°	1	1.5234	1.5234	1.5317	1.5291	1.5276	1.5265	1.5266	1.5256	1.5251	1.5247	1.5254	1.5250	1.5248	1.5245
	2	1.7881	1.7881	1.8038	1.7987	1.7958	1.7939	1.7930	1.7919	1.7911	1.7905	1.7916	1.7918	1.7915	1.7911
	3	3.5251	3.5251	3.5544	3.5476	3.5426	3.5389	3.5392	3.5357	3.5333	3.5315	3.5365	3.5341	3.5325	3.5311
	4	4.7418	4.7418	4.9016	4.8491	4.8205	4.8022	4.7966	4.7790	4.7704	4.7647	4.8025	4.7858	4.7771	4.7713
	5	5.7179	5.7180	5.8014	5.7756	5.7607	5.7509	5.7470	5.7398	5.7352	5.7318	5.7441	5.7401	5.7369	5.7340
	6	6.8856	6.8856	6.9924	6.9634	6.9446	6.9309	6.9202	6.9114	6.9048	6.8995	6.9263	6.9153	6.9084	6.9032
	7	7.0915	7.0915	7.2061	7.1735	7.1526	7.1381	7.1351	7.1231	7.1150	7.1091	7.1298	7.1229	7.1174	7.1125
	8	9.0493	7.4138	9.1478	9.0796	9.0350	9.0030	8.9870	8.9555	8.9375	8.9250	8.9960	8.9694	8.9505	8.9369
30°	1	1.6202	1.6202	1.6321	1.6284	1.6262	1.6248	1.6249	1.6235	1.6227	1.6221	1.6229	1.6224	1.6221	1.6218
	2	2.0784	2.0785	2.0991	2.0924	2.0886	2.0861	2.0854	2.0838	2.0826	2.0817	2.0832	2.0831	2.0826	2.0821
	3	3.7115	3.7115	3.7550	3.7444	3.7370	3.7316	3.7325	3.7277	3.7242	3.7216	3.7264	3.7237	3.7216	3.7198
	4	5.0517	5.0517	5.1242	5.1024	5.0891	5.0803	5.0793	5.0726	5.0677	5.0642	5.0729	5.0712	5.0686	5.0659
	5	5.0707	5.0707	5.2269	5.1796	5.1509	5.1319	5.1363	5.1158	5.1041	5.0962	5.1365	5.1187	5.1077	5.1001
	6	7.0800	7.0800	7.2368	7.1987	7.1712	7.1504	7.1380	7.1241	7.1134	7.1047	7.1310	7.1188	7.1101	7.1030
	7	7.6870	7.6870	7.9216	7.8502	7.8083	7.7801	7.7741	7.7483	7.7332	7.7225	7.7702	7.7486	7.7364	7.7275
	8	8.9317	8.6761	9.1592	9.0876	9.0382	9.0014	8.9888	8.9579	8.9369	8.9209	8.9925	8.9608	8.9406	8.9254
45°	1	1.6894	1.6894	1.7017	1.6980	1.6957	1.6942	1.6945	1.6930	1.6921	1.6915	1.6921	1.6915	1.6911	1.6908
	2	2.2397	2.2397	2.2660	2.2575	2.2525	2.2493	2.2487	2.2465	2.2450	2.2439	2.2457	2.2454	2.2448	2.2441
	3	3.8250	3.8250	3.8738	3.8618	3.8534	3.8473	3.8485	3.8435	3.8396	3.8365	3.8420	3.8390	3.8366	3.8345
	4	4.6812	4.6812	4.7538	4.7321	4.7187	4.7098	4.7089	4.7021	4.6971	4.6934	4.7015	4.7006	4.6983	4.6956
	5	5.1973	5.1973	5.3473	5.3054	5.2777	5.2586	5.2705	5.2486	5.2346	5.2252	5.2671	5.2486	5.2361	5.2272
	6	7.2344	7.2345	7.4337	7.3887	7.3552	7.3297	7.3176	7.2997	7.2861	7.2752	7.2991	7.2868	7.2772	7.2692
	7	8.6974	8.6974	9.0806	8.9594	8.8905	8.8453	8.8367	8.7927	8.7695	8.7539	8.8276	8.7905	8.7701	8.7568
	8	8.7855	8.7855	9.1078	9.0131	8.9520	8.9082	8.8894	8.8566	8.8346	8.8174	8.8880	8.8564	8.8357	8.8201

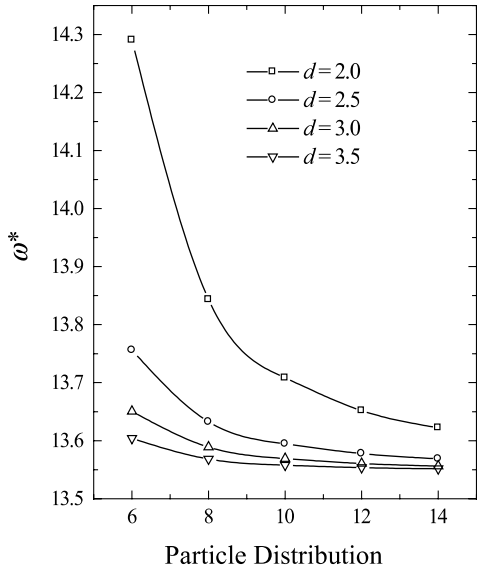

Fig. 2. Convergence characteristics of the frequency parameter ω^* (mode 1) with the particle distribution for a square cylindrical panel ($L/s = 1$, $R/h = 200$).

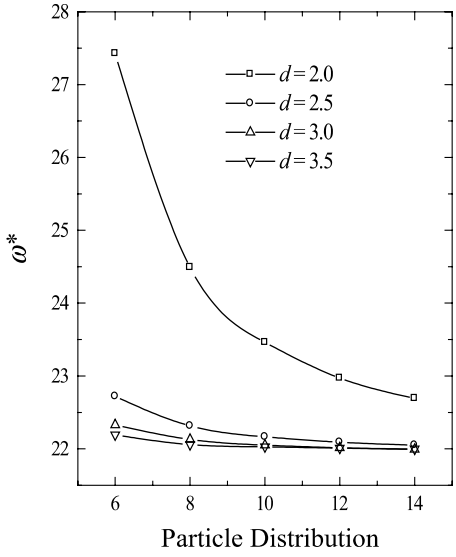

Fig. 3. Convergence characteristics of the frequency parameter ω^* (mode 2) with the particle distribution for a square cylindrical panel ($L/s = 1$, $R/h = 200$).

of rectangular planform. The frequency parameter ω^* used here is defined as $\omega^* = \omega L^2\sqrt{\rho/E_1h^2}$ and the material properties are taken as follows: $E_1 = 138$ GPa, $E_2 = 8.96$ GPa, $G_{12} = 7.1$ GPa, and $v_{12} = 0.3$.

Figs. 6 and 7 present the frequency results for panels with subtended angle of $\theta_0 = 30°$ and four-layer symmetric and anti-symmetric lamination schemes, respectively. For the SSSS case, the fundamental

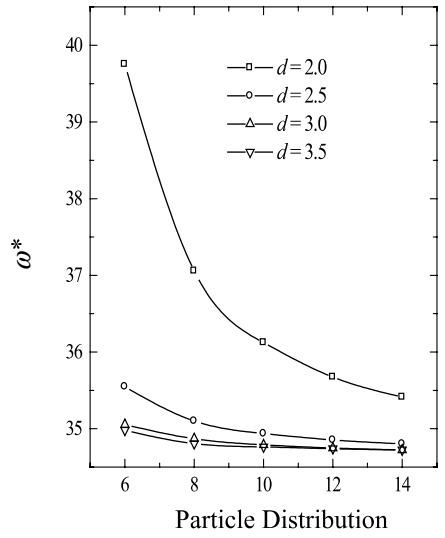

Fig. 4. Convergence characteristics of the frequency parameter ω^* (mode 3) with the particle distribution for a square cylindrical panel ($L/s = 1$, $R/h = 200$).

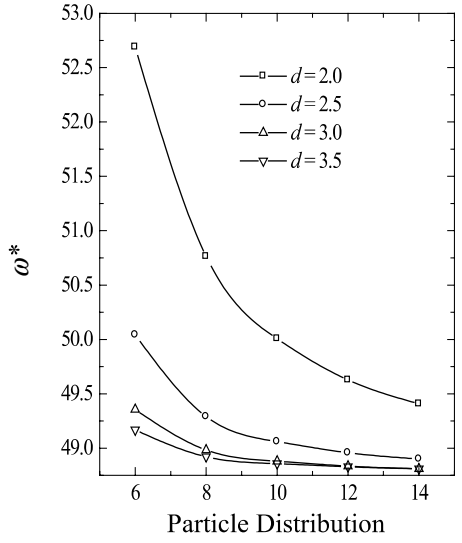

Fig. 5. Convergence characteristics of the frequency parameter ω^* (mode 4) with the particle distribution for a square cylindrical panel ($L/s = 1$, $R/h = 200$).

frequencies of the panel first increase with the lamination angle ϕ until it reaches a maximum at $\phi = 75°$. Subsequently, as ϕ is increased further, the frequencies decrease. For the CFFF case, the fundamental frequencies generally decrease with the increase of the lamination angle ϕ. In the case of the FFFF panel, similar trend to that of the SSSS panel is observed. Here however, the maximum frequencies do not occur at

Table 8
Convergence characteristics of the frequency parameter $\omega^* = \omega L^2\sqrt{12\rho(1-\nu^2)/Eh^2}$ for an isotropic free (FFFF) cylindrical panel ($L/R = 0.5$, $R/h = 200$, $L/b = 1$)

Mode	Particle distribution	$d = 2.0$	$d = 2.5$	$d = 3.0$	$d = 3.5$
1	6×6	14.2904	13.7562	13.6506	13.6039
	8×8	13.8433	13.6324	13.5889	13.5684
	10×10	13.7083	13.5946	13.5691	13.5576
	12×12	13.6516	13.5778	13.5606	13.5535
	14×14	13.6222	13.5687	13.5562	13.5516
2	6×6	27.4271	22.7185	22.3281	22.1904
	8×8	24.4902	22.3144	22.1276	22.0577
	10×10	23.4615	22.1644	22.0501	22.0262
	12×12	22.9711	22.0912	22.0131	22.0093
	14×14	22.6920	22.0494	21.9923	21.9966
3	6×6	39.7523	35.5469	35.0533	34.9786
	8×8	37.0571	35.0997	34.8694	34.8056
	10×10	36.1220	34.9361	34.7891	34.7622
	12×12	35.6727	34.8526	34.7472	34.7388
	14×14	35.4131	34.8025	34.7226	34.7223
4	6×6	52.6900	50.0426	49.3549	49.1681
	8×8	50.7642	49.2905	48.9830	48.9210
	10×10	50.0064	49.0604	48.8801	48.8577
	12×12	49.6282	48.9575	48.8350	48.8283
	14×14	49.4072	48.9003	48.8100	48.8100

Table 9
Convergence characteristics of the frequency parameter $\omega^* = \omega L^2\sqrt{12\rho(1-\nu^2)/Eh^2}$ for an isotropic (SSSS) cylindrical panel ($L/R = 0.5$, $R/h = 200$, $L/b = 1$)

Mode	Particle distribution	$d = 2.0$	$d = 2.5$	$d = 3.0$	$d = 3.5$
1	6×6	69.6968	60.5406	59.1735	59.2010
	8×8	64.5443	59.5386	58.7815	58.7346
	10×10	62.5840	59.2221	58.6992	58.6670
	12×12	61.5691	59.0788	58.6883	58.6735
	14×14	60.9482	59.0021	58.6970	58.6952
3	6×6	119.0492	110.9711	105.7813	103.7097
	8×8	117.2338	105.3944	102.2004	102.0482
	10×10	116.3624	103.3382	101.0083	101.2149
	12×12	115.1580	102.2171	100.4302	100.6841
	14×14	111.8569	101.5218	100.1091	100.3482

similar ϕ for the symmetric and anti-symmetric lamination schemes. For the symmetric scheme, maximum frequency occurs at $\phi = 53°$ while for the anti-symmetric scheme, maximum frequency occurs at $\phi = 48°$. Generally, between the three boundary condition cases, the SSSS case achieves the highest fundamental frequency for any lamination angle ϕ.

Figs. 8 and 9 show the corresponding results for the cases where $\theta_0 = 60°$. For the SSSS case, the maximum frequency occurs at $\phi = 35°$ for the symmetric scheme, and at $\phi = 45°$ for the anti-symmetric

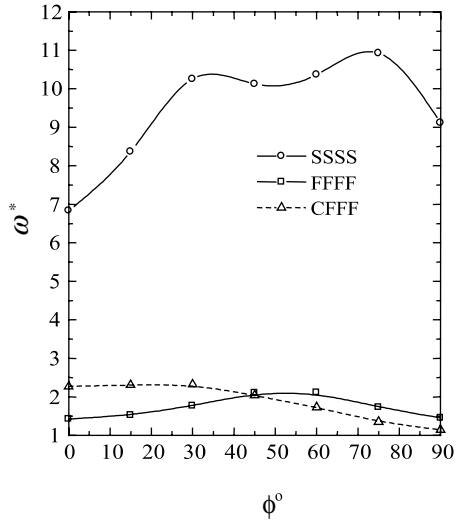

Fig. 6. Variation of frequency parameter ω^* with lamination angle ϕ of a symmetric four-layered cylindrical panel $[\phi - \phi/ - \phi/\phi]$ ($\theta_0 = 30°$, $R/h = 200$, $L/s = 1$).

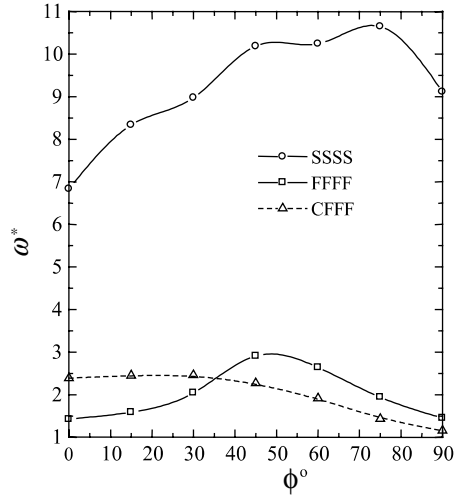

Fig. 7. Variation of frequency parameter ω^* with lamination angle ϕ of an anti-symmetric four-layered cylindrical panel $[\phi/ - \phi/\phi/ - \phi]$ ($\theta_0 = 30°$, $R/h = 200$, $L/s = 1$).

scheme. For the CFFF case, unlike that observed in Figs. 6 and 7, the frequencies here do not generally decrease with increased ϕ. Here, maximum frequency occurs at $\phi = 30°$ for both the symmetric as well as the anti-symmetric schemes. Finally, for the case of the FFFF panel, maximum frequency is observed at $\phi = 70°$ for the symmetric scheme, and for the anti-symmetric scheme, at $\phi = 65°$. As are Figs. 6 and 7, results in Figs. 8 and 9 again show that of the three boundary condition cases considered, the SSSS case generally generates the highest fundamental frequency for any lamination angle ϕ.

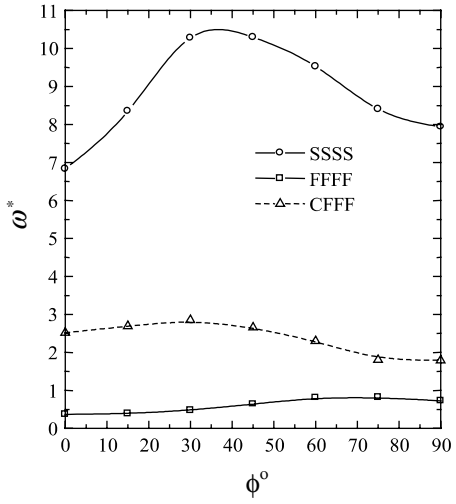

Fig. 8. Variation of frequency parameter ω^* with lamination angle ϕ of a symmetric four-layered cylindrical panel $[\phi/-\phi/-\phi/\phi]$ ($\theta_0 = 60°$, $R/h = 200$, $L/s = 1$).

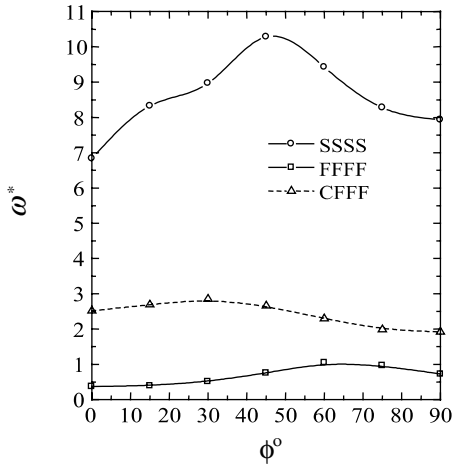

Fig. 9. Variation of frequency parameter ω^* with lamination angle ϕ of an anti-symmetric four-layered cylindrical panel $[\phi/-\phi/\phi/-\phi]$ ($\theta_0 = 60°$, $R/h = 200$, $L/s = 1$).

4. Conclusions

This paper dealt with the free vibration of composite laminated cylindrical panels using two-dimensional reproducing kernel particle approximates. The mathematical formulation for this MFA has been presented. The effects of particle distribution and the size of the domain of influence, on convergence characteristics were investigated. The accuracy of the approach has been validated via extensive comparisons with available published results, with very good agreement observed. The effects of boundary conditions and lamination angles in symmetric and anti-symmetric schemes, on the fundamental frequencies of the panels were also examined in detail. It was found that the effects of the lamination scheme on the frequencies of the panels were different for each of the different boundary conditions considered.

References

Bardell, N.S., Dunsdon, J.N., Langley, R.S., 1997. Free and forced vibration analysis of thin, laminated, cylindrical curved panels. Composite Structures 38, 453–562.

Bercin, A.N., 1996. Natural frequencies of cross-ply laminated singly curved panels. Mechanics Research Communications 23, 165–170.

Chen, J.S., Pan, C., Wu, C.T., Liu, W.K., 1996. Reproducing kernel particle methods for large deformation analysis of non-linear structures. Computer Methods in Applied Mechanics and Engineering 139, 195–227.

Leissa, A.W., 1993. Vibration of Shells. Acoustical Society of American.

Leissa, A.W., Narita, Y., 1984. Vibrations of completely free shallow shells of rectangular planeform. Journal of Sound and Vibration 96, 207–218.

Li, S., Liu, W.K., 1996. Moving least-square reproducing kernel method, part 2: Fourier analysis. Computer Methods in Applied Mechanics and Engineering 139, 159–193.

Liew, K.M., Feng, Z.C., 2000. Vibration characteristics of conical shell panels with three-dimensional flexibility. Transaction of the ASME Journal of Applied Mechanics 67, 314–320.

Liew, K.M., Bergman, L.A., Ng, T.Y., Lam, K.Y., 2000. Three-dimensional vibration of cylindrical shell panels-solution by continuum and discrete approaches. Computational Mechanics 26, 208–221.

Liew, K.M., Wu, H.Y., Ng, T.Y., 2002a. Meshless method for modeling of human proximal femur: treatment of nonconvex boundaries and stress analysis. Computational Mechanics 28, 390–400.

Liew, K.M., Wu, Y.C., Zou, G.P., Ng, T.Y., 2002b. Elasto-plasticity revisited: numerical analysis via reproducing kernel particle method and parametric quadratic programming. International Journal for Numerical Methods in Engineering 55, 669–683.

Liew, K.M., Ng, T.Y., Wu, Y.C., 2002c. Meshfree method for large deformation analysis a reproducing kernel particle method. Engineering Structures 24, 51–58.

Liew, K.M., Ng, T.Y., Zhao, X., Reddy, J.N., 2002d. Harmonic reproducing kernel particle method for free vibration analysis of rotating cylindrical shells. Computer Methods in Applied Mechanics and Engineering 191, 4141–4157.

Liu, W.K., Jun, S., Zhang, Y.F., 1995a. Reproducing kernel particle methods. International Journal of Numerical Methods in Fluids 20, 1081–1106.

Liu, W.K., Jun, S., Li, S., Adee, J., Belytschko, T., 1995b. Reproducing kernel particle methods for structural dynamics. International Journal for Numerical Methods in Engineering 38, 1655–1679.

Liu, W.K., Li, S., Belytschko, T., 1997. Moving least-square reproducing kernel methods, part 1: Methodology and convergence. Computer Methods in Applied Mechanics and Engineering 143, 113–154.

Lucy, L.B., 1977. A numerical approach to the testing the fission hypothesis. The Astrophysical Journal 82, 1013–1024.

Messina, A., Soldatos, K.P., 1999. Vibration of completely free composite plates and cylindrical shell panels by a higher-order theory. International Journal of Mechanical Sciences 41, 891–918.

Monaghan, J.J., 1988. An introduction to SPH. Computer Physics Communications 48, 89–96.

Nagashima, T., 1999. Node-by-node meshless approach and its application to structural analysis. International Journal for Numerical Methods in Engineering 46, 341–385.

Ouatouati, A.E.L., Johnson, D.A., 1999. A new approach for numerical modal analysis using the element-free method. International Journal for Numerical Methods in Engineering 46, 1–27.

Qatu, M.S., 1991. Free vibrations of laminated composite rectangular plates. International Journal of Solids and Structures 28, 941–954.

Qatu, M.S., Leissa, A.W., 1991. Free vibrations of completely free doubly curved laminated composite shallow shells. Journal of Sound and Vibration 151, 9–29.

Qatu, M.S., 1992. Mode shape analysis of angle-ply laminated composite shallow shells. Journal of the Acoustics Society of America 92, 1509–1520.

Soldatos, K.P., 1984. A comparison of some shell theories used for the dynamic analysis of cross-ply laminated circular cylindrical panels. Journal of Sound and Vibration 97, 305–319.

Soldatos, K.P., Hadjigeorgiou, V.P., 1990. Three-dimensional solution of the free vibration problem of homogeneous isotropic cylindrical shells and panels. Journal of Sound and Vibration 137, 369–384.

Soldatos, K.P., Messina, A., 2001. The influence of boundary conditions and transverse shear on the vibration of angle-ply laminated plates, circular cylinders and cylindrical panels. Computer Method in Applied Mechanics and Engineering 190, 2385–2409.